

Delocalization of topological surface states by diagonal disorder in nodal loop semimetals

João Silva,¹ Miguel A. N. Araújo,^{2,3,4} Miguel Gonçalves,² Pedro Ribeiro,^{2,4} and Eduardo V. Castro^{1,4}

¹*Centro de Física das Universidades do Minho e Porto,
Departamento de Física e Astronomia, Faculdade de Ciências,
Universidade do Porto, 4169-007 Porto, Portugal*

²*CeFEMA, Instituto Superior Técnico, Universidade de Lisboa, Av. Rovisco Pais, 1049-001 Lisboa, Portugal*

³*Departamento de Física, Universidade de Évora, P-7000-671, Évora, Portugal*

⁴*Beijing Computational Science Research Center, Beijing 100084, China*

The effect of Anderson diagonal disorder on the topological surface (“drumhead”) states of a Weyl nodal loop semimetal is addressed. Since diagonal disorder breaks chiral symmetry, a winding number cannot be defined. Seen as a perturbation, the weak random potential mixes the clean exponentially localized drumhead states of the semimetal, thereby producing two effects: (i) the algebraic decay of the surface states into the bulk; (ii) a broadening of the low energy density of surface states of the open system due to degeneracy lifting. This behavior persists with increasing disorder, up to the bulk semimetal-to-metal transition at the critical disorder W_c . Above W_c , the surface states hybridize with bulk states and become extended into the bulk.

I. INTRODUCTION

The most appealing property of topological matter is the robustness of certain material properties to perturbations. Among such properties, the creation of robust localized states at the edge or surface of a sample is probably the most striking. Rooted in the bulk-edge correspondence, these topologically protected edge states survive weak disorder, which makes them appealing also from the point of view of applications. Three dimensional (3D) topological insulators, with their two-dimensional (2D) Dirac-fermions at the surface, stood out as an important class of topological materials [1, 2] whose stability with respect to interactions and disorder is by now fairly well established [3, 4]. Gapless systems can, however, also support non-trivial momentum-space topology and robust, topologically protected, surface states. Among these are the Weyl nodal loop (WNL) semimetals, for which the valence and conduction bands linearly touch along one-dimensional (1D) loops in 3D momentum space [5]. Their recent theoretical prediction [6–9] and experimental discovery [10, 11] triggered intense experimental [12–18] and theoretical interest [19–33].

The WNL’s topological nature manifests itself by the presence of localized (“drumhead”) states [7, 22, 34–36]. In the thermodynamic limit, the surface states have zero energy and produce a delta-function contribution to the bulk density of states (DOS) of the open system, $\rho_{\text{edge}}(E) \propto A_{\bullet} \delta(E)$, where A_{\bullet} denotes the \mathbf{k} -space area of the nodal loop projected onto the surface. This has to be contrasted with the bulk density of states: since the Fermi surface is reduced to a 1D nodal line, the bulk DOS, $\rho_{\text{bulk}}(E)$, vanishes linearly for low energies, i.e. $\rho_{\text{bulk}}(E) \propto |E|$. Drumhead states have already been observed experimentally through angle-resolved photoemission spectroscopy (ARPES), transport measurements and de Haas–van Alphen quantum oscillations [18, 37–

41].

The effect of static disorder on the bulk properties has been addressed recently [42]. Within an Anderson model of box-distributed disorder, a phase transition was found from a bulk low disorder multifractal semimetallic (SM) phase, where the momentum-space wave-function has multifractal structure, to a single-fractal diffusive metallic (M) phase. This SM/M transition takes place at a finite disorder value, W_c [43].

For a WNL, the fate of the topological drumhead states under finite disorder is yet unknown. To our knowledge, only the effect of an incommensurate potential on the drumhead states of a nodal link semimetal has been addressed [44]. However, that work assumed the potential to depend only on one spatial coordinate, while translational invariance in the perpendicular plane was preserved. A study of three-dimensional disorder effects on the surface states of a WNL is in order, then.

In this work, we unveil the fate of the topological surface states of the open WNL system under Anderson short ranged diagonal disorder. Because the latter breaks chiral symmetry, a winding number cannot be defined. However, the surface states can be detected by studying (i) the density of surface states (DOSS), $\Delta\rho(E)$, defined as the change in the DOS when a surface is created in the direction perpendicular to the nodal loop plane; and (ii) the localization properties of the topological surface states with increasing disorder.

The rest of the paper is organized as follows. In Sec. II we present the model and provide details on the methods used in this work. The results are given in Sec. III. In Sec IV a final discussion is provided.

II. MODEL AND METHODS

We study a two-band model of a WNL system on a cubic lattice with diagonal disorder,

$$H = \sum_{\mathbf{k}} c_{\mathbf{k}}^{\dagger} H_{\mathbf{k}} c_{\mathbf{k}} + \sum_{\mathbf{r}} c_{\mathbf{r}}^{\dagger} V_{\mathbf{r}}(W) c_{\mathbf{r}}. \quad (1)$$

The first term describes a clean WNL semimetal [42], with \mathbf{k} a 3D Bloch vector, $H_{\mathbf{k}} = (t_x \cos k_x + t_y \cos k_y + \cos k_z - m)\tau_x + t_2 \sin k_z \tau_y$, with τ_x, τ_y Pauli matrices acting on the orbital pseudo-spin indices $\alpha = 1, 2$, and $c_{\mathbf{k}}^{\dagger} = (c_{\mathbf{k},1}^{\dagger} \ c_{\mathbf{k},2}^{\dagger})$, where $c_{\mathbf{k},\alpha}^{\dagger}$ creates an electron with Bloch momentum \mathbf{k} in the sublattice spanned by α orbitals. The second term is the disorder potential, where \mathbf{r} denotes a lattice site and $V_{\mathbf{r}}(W) = \text{diag}(v_{\mathbf{r}1}, v_{\mathbf{r}2})$, with random variables $v_{\mathbf{r}\alpha} \in [-W/2, W/2]$, where W corresponds to the disorder strength. We ensure that $v_{\mathbf{r}\alpha}$ averages to zero in sublattice $\alpha = 1, 2$ for each disorder realization. The results presented hereafter are for $t_x = 1.1$, $t_y = 0.9$, $m = 2.12$ and $t_2 = 0.8$. The hopping anisotropy chosen breaks unwanted degeneracies and ensures the system is generic within this class. This parameter choice yields a single nodal line, in the $k_z = 0$ plane, given by:

$$t_x \cos k_x + t_y \cos k_y + 1 - m = 0. \quad (2)$$

Because the diagonal disorder breaks chiral symmetry, a winding number cannot be defined. However, the surface states can be detected by studying the DOSS, $\Delta\rho(E)$, defined as $\Delta\rho(E) \equiv \rho_{\text{open}}(E) - \rho_{\text{bulk}}(E)$. Here, ρ_{bulk} denotes the DOS calculated for periodic boundary conditions (PBC), and ρ_{open} denotes the DOS calculated using open boundary conditions (OPB) along the z direction (perpendicular to the nodal loop plane). To compute the DOS we use the kernel polynomial method (KPM) with an expansion in Chebyshev polynomials to order N_m [45, 46], reaching system sizes containing up to $L = 100$ unit cells in each direction.

Exact diagonalization (ED) using the Lanczos method allows us to study the localization properties of the topological surface states. The surface states' localization along the z direction is revealed by an inverse participation ratio defined for the z direction in sublattice α as

$$\text{IPR}_z^{\alpha} = \frac{\sum_z \Psi^4(z, \alpha)}{[\sum_z \Psi^2(z, \alpha)]^2}, \quad (3)$$

with

$$\Psi^2(z, \alpha) = \sum_{x,y} |\psi(x, y, z; \alpha)|^2, \quad (4)$$

where $\psi(x, y, z; \alpha)$ is the eigenstate amplitude in the lattice cell at (x, y, z) and orbital α .

III. RESULTS

A. Clean system

For a better understanding of the effect of diagonal disorder on drumhead surface states, we first review the clean system. Let us write the momentum as $\mathbf{k} = (\mathbf{k}_{\parallel}, k_z)$, where $\mathbf{k}_{\parallel} = (k_x, k_y)$ is the momentum component parallel to the surface. A winding number for each \mathbf{k}_{\parallel} can be defined [34, 47],

$$\begin{aligned} \nu(\mathbf{k}_{\parallel}) &= \frac{1}{2\pi} \int_{-\pi}^{\pi} dk_z \langle \psi(\mathbf{k}_{\parallel}) | \partial_{k_z} | \psi(\mathbf{k}_{\parallel}) \rangle \\ &= \frac{1}{2\pi} \int_{-\pi}^{\pi} \frac{\partial \log H_{12}(\mathbf{k}_{\parallel}, k_z)}{\partial k_z} dk_z, \end{aligned} \quad (5)$$

where $H_{12} = t_x \cos k_x + t_y \cos k_y + \cos k_z - m - it_2 \sin k_z$ is the off-diagonal matrix element of the clean WNL Bloch Hamiltonian. Appealing to dimensional reduction, one can take \mathbf{k}_{\parallel} as a label for a topological chain [48, 49] along the z direction.

Equation (5) yields $\nu(\mathbf{k}_{\parallel}) = 1$ or $\nu(\mathbf{k}_{\parallel}) = 0$ if \mathbf{k}_{\parallel} is inside or outside the nodal loop, respectively. This implies that for each \mathbf{k}_{\parallel} inside the loop, there is a zero-energy surface state $\psi_{\mathbf{k}_{\parallel}}(\mathbf{r}, \alpha = 1) = e^{i(k_x x + k_y y)} \phi_{\mathbf{k}_{\parallel}}(z)$, occupying sublattice $\alpha = 1$, where $\phi_{\mathbf{k}_{\parallel}}(z)$ decays exponentially from the surface at $z = 1$ of a semi-infinite system, $z \geq 1$. For a finite system with linear size L , a similar surface state exists on the opposite surface, $z = L$, occupying sublattice $\alpha = 2$. In the thermodynamic limit, such states have zero energy. For finite L , the small hybridization between drumhead states in opposite surfaces lifts their degeneracy. As \mathbf{k}_{\parallel} approaches the nodal line, the decay length of $\phi_{\mathbf{k}_{\parallel}}(z)$ diverges, thereby increasing the finite-size hybridization.

The number of surface states (p) created by opening a cubic system at $z = 1$ and $z = L$ is just twice the number of \mathbf{k}_{\parallel} points inside the nodal line in Eq. (2), and is thus proportional to the loop area (A_{\bullet}) in \mathbf{k}_{\parallel} -space times L^2 ,

$$p = \Lambda L^2, \quad (6)$$

where we have defined $\Lambda \equiv A_{\bullet}/2\pi^2$. Since the DOS is defined per unit volume, the clean system's DOSS in the $L \rightarrow \infty$ limit is

$$\Delta\rho(E) = \Lambda L^{-1} \delta(E) + f_{\text{reg}}(E), \quad (7)$$

where the δ -function accounts for the topological zero-energy surface states and $f_{\text{reg}}(E)$ is a regular function. The number of zero-energy drumhead states may then be obtained from $\Delta\rho(E)$,

$$p = L^3 \int_{0^-}^{0^+} \Delta\rho(E) dE = \Lambda L^2. \quad (8)$$

Note that for a given system size, the creation of edge states removes states from the bulk and $\int_{-\infty}^{\infty} \Delta\rho(E) dE = 0$.

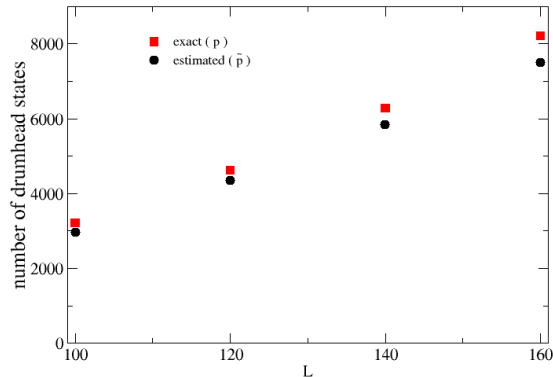


FIG. 1. Clean system’s exact (p , red) and estimated (\tilde{p} , black) number of surface states for different system sizes containing L^3 unit cells. $N_m = 2^{10}$.

Although the clean WNL is analytically tractable, it can serve as a test bed for the DOS calculation through the numerical KMP method. The finiteness of L necessarily causes some broadening of the delta function due to the hybridization explained above. Therefore, one must integrate $\Delta\rho(E)$ over an energy interval in order to obtain the number of edge states, p . The best choice is to define an energy window, E_w , such that $\Delta\rho(E) > 0$ for $|E| < E_w$ and numerically estimate the number of surface states as

$$\tilde{p} = L^3 \int_{-E_w}^{E_w} \Delta\rho(E) dE, \quad (9)$$

which can be compared to the exact value, p . In Tab. I we collect a few examples of p and \tilde{p} . An analogous comparison between p and \tilde{p} as functions of system size L^3 is shown in Fig. 1. The integral in Eq. (9) nearly captures the exact number of edge states, though a finite difference persists even for the larger sizes.

$L_x \times L_y \times L_z$	p	\tilde{p}
$80 \times 80 \times 80$	2050	1965 (96%)
$80 \times 80 \times 160$	2050	1970 (96%)
$80 \times 80 \times 200$	2050	1974 (96%)
$80 \times 80 \times 240$	2050	1978 (96%)
$100 \times 100 \times 100$	3214	3104 (97%)

TABLE I. Clean system’s exact (p) and estimated (\tilde{p}) number of surface states. L_μ corresponds to the number of unit cells in direction $\mu = x, y, z$. In brackets, \tilde{p}/p is given in percentage. The number of polynomials is $N_m = \{2^{11}, 2^{12}\}$.

As stated before, the difference $p - \tilde{p}$ is due to hybridization between edge states on opposite sides of the

sample when \mathbf{k}_\parallel lies close to the nodal line in Eq. (2). The energy splitting displaces some states to outside of the energy window E_w . We expect that the hybridization effect is reduced when the system’s size along z is increased, allowing more states to get captured by Eq. (9), but the effect is relatively small, as Tab. I shows.

B. Disordered system

1. Spectral properties

Anderson disorder, however weak, has two effects: (i) chiral symmetry breaking, and (ii) hybridization between the clean system’s drumhead states.

(i) Because of chiral symmetry breaking, a winding number cannot be defined. The winding number calculated from the eigenstates (Zak phase) in Eq. (5) is not quantized for a system without chiral symmetry and therefore it cannot measure the number of edge states. This holds true for the real space formulation of the Zak phase - the correct formulation for systems with broken translational invariance - where \mathbf{k} can be replaced by phase twists θ in Eq. (5) [50].

(ii) Due to hybridization between all the clean system’s drumhead states, their energies are shifted, causing a disorder broadening of the DOSS near zero energy. An example of the DOSS broadening around $E = 0$, averaged over disorder realizations, is shown in Fig. 2, where the smallest disorder considered is $W = 1$, much smaller than the bandwidth of the clean system.

Under increasing disorder strength, W , the energy window, E_w , of Eq. (9) also increases. This is seen in Fig. 2, where a notable $\Delta\rho(E) > 0$ for an increasing energy window around $E = 0$ is present even for $W = 4$. These results suggest that some sort of edge states, reminiscent of the topological drumhead states, persist at higher disorder, even though topological protection is not at work due to chiral symmetry breaking. In Sec. III B 2 we provide details on the localization properties of these edge states.

It should be noted that for $W \gtrsim 2.6$, the bulk develops a nonzero $\rho_{\text{bulk}}(0)$, entering the metallic diffusive phase [42]. For $W > 6$ the DOS around zero energy no longer resembles that of a semimetallic WNL, which is characterized by a linearly vanishing DOS. In our model, the linear dependence occurs in an energy scale $|E| \lesssim 0.8$ [42]. For $W > 6$ we obtain $E_w \gtrsim 0.8$, therefore, larger than the energy scale characterizing a WNL in the semimetal phase. This means that $W = 6$ is a very strong disorder. Incidentally, we note that at $E = 0$, Anderson localization in this model occurs for a much stronger disorder of $W_A \approx 11$ [42].

The integrated DOSS in the energy window E_w , i.e. \tilde{p} in Eq. (9), is shown in Fig. 3 as function of disorder strength. Because Eq. (7) suggests a L^{-1} scaling of the

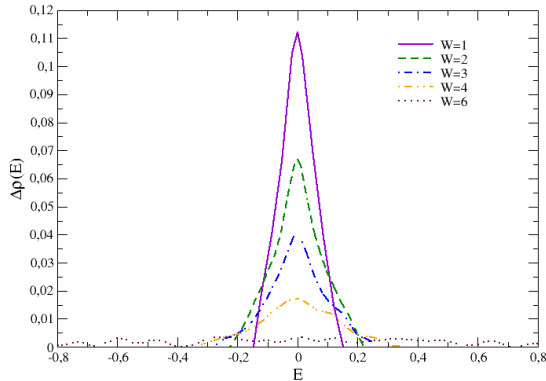


FIG. 2. Averaged DOSS, $\langle \Delta\rho(\epsilon) \rangle > 0$, in an energy window E_w that grows with increasing W , for $L = 100$. The average is over 20 disorder realizations.

DOSS, in Fig. 3 we plot the L -rescaled data. The different data for $L\tilde{\rho}$ seem to collapse in a single curve, approximately linear, suggesting an exponential decay of the number of surface states. For high disorder, $W > 6$, there are strong fluctuations, pointing to a negligible edge signal for such high disorder values. A fit to the $L = 200$ data yields the number of surface states scaling as $\tilde{\rho} \propto L^2 \exp(-0.44W)$ in the range $W \in [1, 6]$. The number of edge states is a monotonically decreasing function of W , in contrast to the chiral off-diagonal disorder case, where an enhancement of the number of surface states has been found for small disorder, up to $W \approx 1.75$ [51].

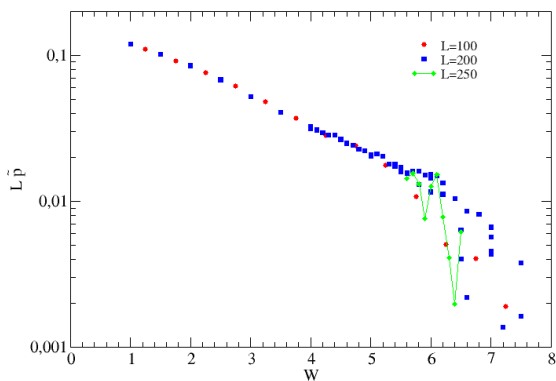


FIG. 3. Logarithmic plot of $L\tilde{\rho}$ for different L . A reasonable collapse is observed for $W < 6$, indicating L^{-1} scaling. For $W > 6$ the collapse of the curves is not clear.

In a clean WNL, the drumhead states are labeled by \mathbf{k}_{\parallel} , which is a good quantum number. The (exponential)

decay length into the bulk depends on \mathbf{k}_{\parallel} and diverges as \mathbf{k}_{\parallel} approaches the nodal line. As stated above, any small amount of disorder mixes the clean drumhead states of a WNL: the \mathbf{k}_{\parallel} labeling of the surface states loses its meaning. However, the surface states projection onto a plane wave state \mathbf{k}_{\parallel} in the plane $z = 1$ for sublattice $\alpha = 1$ can be probed by computing the local DOS on the state

$$|\psi\rangle \equiv |z = 1, k_x, k_y = 0\rangle = \sum_{x,y} e^{ik_x x} |x, y, z = 1, \alpha = 1\rangle, \quad (10)$$

at energy $E = 0$, defined as

$$\Delta\rho(z = 1, k_x, k_y = 0, E = 0) \equiv \sum_{j(\text{open})} |\langle \psi | j \rangle|^2 \delta(E_j) - \sum_{j(\text{closed})} |\langle \psi | j \rangle|^2 \delta(E_j) \quad (11)$$

where j runs over all quantum eigenstates of the open or closed system. The state in Eq. (10) is localized at the $z = 1$ plane and therefore the LDOS in it should be large for surface states.

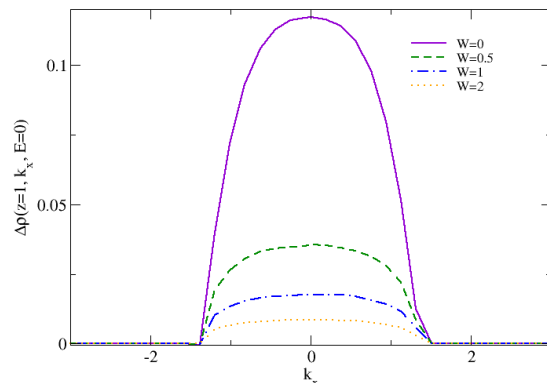


FIG. 4. LDOS on the state defined in Eq. (10) for $L = 100$, averaged over 40 disorder realizations.

The result for the LDOS in state (10) is plotted in Fig. 4. It implies that the surface states contain high weight on the state in Eq. (10) in the region inside the nodal loop. The corresponding quantity for the clean system is shown for comparison. Clearly, a reminiscence of the nodal line remains for $W = 1$. We note that the KPM calculated DOS value at $E = 0$ depends on the bandwidth, which increases with W . This implies that the energy resolution of the calculation is different for different W [46]. Therefore, only the widths of the curves in figure 4 can be accurately compared, not their absolute values.

2. Localization properties

Because of disorder mixing, one can simulate the resulting surface states as linear superpositions of the clean system's drumhead states with random coefficients. This yields states that decay algebraically into the bulk. A realistic calculation of the surface wave function confirms this expectation. We used Lanczos ED to find a number of low energy states and calculate the surface state probability along z , as defined in Eq. (4), projected on sublattice $\alpha = 1$. It is seen that the probability indeed decays as a power law into the bulk, even for small disorder. This is shown in Fig. 5 for $W = 0.5$. A fit to $\Psi^2(z, \alpha) \sim z^{-\nu}$ gives $\nu = 1.8$, which implies an integrable probability as expected for localized states. Hybridization with the surface state localized in the opposite boundary is seen for $z > 20$. Similar behavior is found for the other low energy states. By projecting on sublattice $\alpha = 2$, we find similar decaying states from the surface $z = L$, as expected.

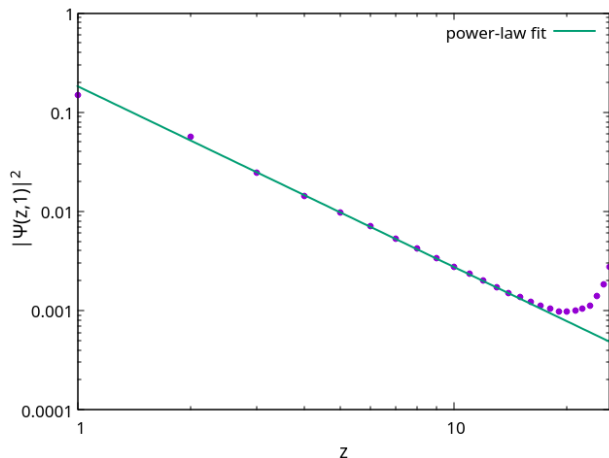


FIG. 5. Log-log plot of eigenstate's probability projected onto sublattice $\alpha = 1$, for the state with energy closest to $E = 0$, for $L = 26$ and $W = 0.5$. The probability decays approximately as $z^{-1.8}$ into the bulk.

One of the basic principles of the theory of Anderson localization is that there cannot be two different localization lengths at the same energy. Since a WNL semimetal has $\rho_{\text{bulk}}(E) \propto |E|$, at finite energy the drumhead states must hybridize with the extended bulk states and become *delocalized*. Therefore, a low energy surface state should have the following properties: retain high probability near the surface, show power-law decay into the bulk, and become extended further into the bulk. At strictly zero energy, there are no bulk states to hybridize with. This is valid up to the amount of disorder that renders $\rho_{\text{bulk}}(0)$ finite, $W \gtrsim 2.6$ [42]. Then, a zero energy "surface" state becomes fully extended. Evidence for this behavior is shown in Fig. 6. It shows IPR_z^α for sublattice $\alpha = 1$, as defined in Eq. (3), which allows us to study the

wave function localization along the z axis. For extended states in one dimension, the inverse participation ratio scales with the inverse of the system's size, L^{-1} . Such a scaling is observed in Fig. 6, where results for different system sizes are plotted. The L -rescaled data collapse into a single curve for $W \gtrsim 2.6$, thus corroborating the above picture.

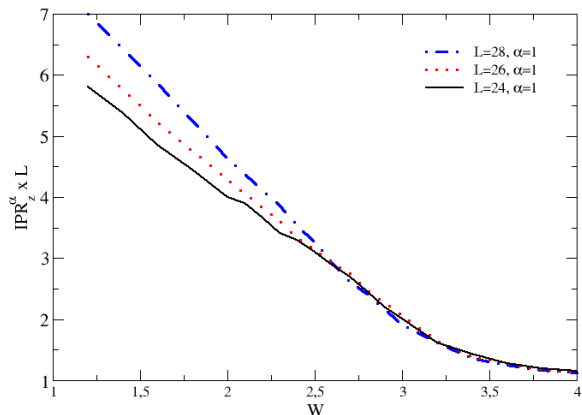


FIG. 6. IPR_z^α for $L = 24$ – 28 and the two eigenstates closer to $E = 0$, averaged over 400 disorder realizations.

IV. DISCUSSION

We have explored the fate of topological drumhead surface states due to disorder of the Anderson type in the WNL semimetal. Because of chiral symmetry breaking, a quantized topological index (winding number) providing the number of edge states does not exist, as opposed to the clean case. However, in the presence of disorder, a finite sample along z – the direction perpendicular to the loop plane – contains extra states close to zero energy, as compared to the infinite system. Such states have high probability close to the surface and decay algebraically into the bulk. Since there is no chiral symmetry, these states can occur at finite energies ($E \neq 0$) due to disorder broadening, and extend into the bulk because of hybridization with bulk states, which have finite bulk DOS in the semimetallic phase. A similarity can be drawn, here, to the *virtual bound state* concept in the non-interacting Anderson impurity problem: an initially localized impurity state retains high probability close to the impurity but is plane-wave-like far away due to hybridization with the Bloch band.

At high enough disorder, above the semimetal to metal transition found in Ref. [42], even the $E = 0$ surface states become extended because the bulk DOS, $\rho_{\text{bulk}}(0)$, becomes finite with bulk metallic states. Surface creation

brings about an exponentially decreasing number of extended low energy states, up to very high disorder. The number of such states is also proportional to the area of the sample. This is the leftover of the clean WNL semimetal topology.

Some materials have been confirmed to host nodal lines [18, 37, 38, 52–55]. ARPES and transport properties have been used to probe these materials and also nodal line semimetal candidates [40, 56]. An interesting direction for future study is to understand the signatures of the disorder-driven power-law decaying surface states here unveiled in ARPES and transport.

The authors MA, MG and PR acknowledge partial support from Fundação o para a Ciência e Tecnologia (Portugal) through Grant No. UID/CTM/04540/2019. JS and EVC acknowledge partial support from Fundação para a Ciência e Tecnologia (FCT-Portugal) through Grant No. UIDB/04650/2020. MG acknowledges further support from FCT-Portugal through the Grant SFRH/BD/145152/2019.

-
- [1] M. Z. Hasan and C. L. Kane, *Rev. Mod. Phys.* **82**, 3045 (2010).
- [2] X.-L. Qi and S.-C. Zhang, *Rev. Mod. Phys.* **83**, 1057 (2011).
- [3] C. K. Chiu, J. C. Teo, A. P. Schnyder, and S. Ryu, *Rev. Mod. Phys.* **88**, 035005 (2016).
- [4] S. Rachel, *Reports Prog. Phys.* **81**, 116501 (2018).
- [5] N. P. Armitage, E. J. Mele, and A. Vishwanath, *Rev. Mod. Phys.* **90**, 015001 (2018).
- [6] Y. Kim, B. J. Wieder, C. L. Kane, and A. M. Rappe, *Phys. Rev. Lett.* **115**, 036806 (2015).
- [7] H. Weng, Y. Liang, Q. Xu, R. Yu, Z. Fang, X. Dai, and Y. Kawazoe, *Phys. Rev. B* **92**, 045108 (2015).
- [8] K. Mullen, B. Uchoa, and D. T. Glatzhofer, *Phys. Rev. Lett.* **115**, 26403 (2015).
- [9] Y. Chen, Y. Xie, S. A. Yang, H. Pan, F. Zhang, M. L. Cohen, and S. Zhang, *Nano Lett.* **15**, 6974 (2015).
- [10] L. S. Xie, L. M. Schoop, E. M. Seibel, Q. D. Gibson, W. Xie, and R. J. Cava, *APL Mater.* **3**, 083602 (2015).
- [11] G. Bian, T.-R. Chang, R. Sankar, S.-Y. Xu, H. Zheng, T. Neupert, C.-K. Chiu, S.-M. Huang, G. Chang, I. Belopolski, D. S. Sanchez, M. Neupane, N. Alidoust, C. Liu, B. Wang, C.-C. Lee, H.-T. Jeng, C. Zhang, Z. Yuan, S. Jia, A. Bansil, F. Chou, H. Lin, and M. Z. Hasan, *Nat. Commun.* **7**, 10556 (2016).
- [12] L. M. Schoop, C. Straßer, A. Topp, V. Duppel, B. V. Lotsch, C. R. Ast, M. N. Ali, S. S. P. Parkin, A. Varykhalov, and D. Marchenko, *Nat. Commun.* **7**, 11696 (2016).
- [13] Y. Okamoto, T. Inohara, A. Yamakage, Y. Yamakawa, and K. Takenaka, *J. Phys. Soc. Japan* **85**, 123701 (2016).
- [14] C. Q. Xu, W. Zhou, R. Sankar, X. Z. Xing, Z. X. Shi, Z. D. Han, B. Qian, J. H. Wang, Z. Zhu, J. L. Zhang, A. F. Bangura, N. E. Hussey, and X. Xu, *Phys. Rev. Mater.* **1**, 064201 (2017).
- [15] R. Lou, P. Guo, M. Li, Q. Wang, Z. Liu, S. Sun, C. Li, X. Wu, Z. Wang, Z. Sun, D. Shen, Y. Huang, K. Liu, Z.-Y. Lu, H. Lei, H. Ding, and S. Wang, *npj Quantum Mater.* **3**, 43 (2018).
- [16] A. Laha, S. Mallick, R. Singha, P. Mandal, P. Rambabu, V. Kanchana, and Z. Hossain, *Phys. Rev. B* **99**, 241102 (2019).
- [17] Z. Qiu, C. Le, Z. Liao, B. Xu, R. Yang, J. Hu, Y. Dai, and X. Qiu, (2019), [arXiv:1904.01811](https://arxiv.org/abs/1904.01811).
- [18] C. Sims, M. M. Hosen, H. Aramberri, C.-Y. Huang, G. Dhakal, K. Dimitri, F. Kabir, S. Regmi, X. Zhou, T.-R. Chang, H. Lin, D. Kaczorowski, N. Kioussis, and M. Neupane, (2019), [arXiv:1906.09642](https://arxiv.org/abs/1906.09642).
- [19] J.-W. Rhim and Y. B. Kim, *Phys. Rev. B* **92**, 045126 (2015).
- [20] C. Fang, Y. Chen, H.-Y. Kee, and L. Fu, *Phys. Rev. B* **92**, 081201 (2015).
- [21] H. Huang, J. Liu, D. Vanderbilt, and W. Duan, *Phys. Rev. B* **93**, 201114 (2016).
- [22] Y.-H. Chan, C.-K. Chiu, M. Y. Chou, and A. P. Schnyder, *Phys. Rev. B* **93**, 205132 (2016).
- [23] J.-L. Lu, W. Luo, X.-Y. Li, S.-Q. Yang, J.-X. Cao, X.-G. Gong, and H.-J. Xiang, *Chinese Phys. Lett.* **34**, 057302 (2017).
- [24] Q. Xu, R. Yu, Z. Fang, X. Dai, and H. Weng, *Phys. Rev. B* **95**, 045136 (2017).
- [25] Y. Du, X. Bo, D. Wang, E.-j. Kan, C.-G. Duan, S. Y. Savrasov, and X. Wan, *Phys. Rev. B* **96**, 235152 (2017).
- [26] J. Liu and L. Balents, *Phys. Rev. B* **95**, 075426 (2017).
- [27] L. Oroszlány, B. Dóra, J. Cserti, and A. Cortijo, *Phys. Rev. B* **97**, 205107 (2018).
- [28] A. Martín-Ruiz and A. Cortijo, *Phys. Rev. B* **98**, 155125 (2018).
- [29] Y. Wang, H. Hu, and S. Chen, *Phys. Rev. B* **98**, 205410 (2018).
- [30] A. Lau and C. Ortix, *Phys. Rev. Lett.* **122**, 186801 (2019).
- [31] M. Ezawa, *Sci. Rep.* **9**, 5286 (2019).
- [32] L. Li and M. A. N. Araújo, *Phys. Rev. B* **94**, 165117 (2016).
- [33] L. Li, H. H. Yap, M. A. N. Araújo, and J. Gong, *Phys. Rev. B* **96**, 235424 (2017).
- [34] M. Araújo and P. Sacramento, *Topology In Condensed Matter: An Introduction* (World Scientific Publishing Company, 2021).
- [35] A. A. Burkov, M. D. Hook, and L. Balents, *Phys. Rev. B* **84**, 235126 (2011).
- [36] D. W. Zhang, Y. X. Zhao, R. B. Liu, Z. Y. Xue, S. L. Zhu, and Z. D. Wang, *Phys. Rev. A* **93**, 043617 (2016).
- [37] L. M. Schoop, M. N. Ali, C. Straßer, A. Topp, A. Varykhalov, D. Marchenko, V. Duppel, S. S. P. Parkin, B. V. Lotsch, and C. R. Ast, *Nat. Comm.* **7**, 11696 (2016).
- [38] T. Nakamura, S. Souma, Z. Wang, K. Yamauchi, D. Takane, H. Oinuma, K. Nakayama, K. Horiba, H. Kumigashira, T. Oguchi, T. Takahashi, Y. Ando, and T. Sato, *Phys. Rev. B* **99**, 245105 (2019).
- [39] I. Belopolski, K. Manna, D. S. Sanchez, G. Chang, B. Ernst, J. Yin, S. S. Zhang, T. Cochran, N. Shumiya, H. Zheng, B. Singh, G. Bian, D. Multer, M. Litskevich, X. Zhou, S.-M. Huang, B. Wang, T.-R. Chang, S.-Y. Xu, A. Bansil, C. Felser, H. Lin, and M. Z. Hasan, *Science* **365**, 1278 (2019), [arXiv:2004.00004](https://arxiv.org/abs/2004.00004).
- [40] M. Hosen, G. Dhakal, B. Wang, N. Poudel, K. Dimitri, F. Kabir, C. Sims, S. Regmi, K. Gofryk, D. Kaczorowski,

- A. Bansil, and M. Neupane, *Scientific Reports* **10**, 2776 (2020).
- [41] B. A. Stuart, S. Choi, J. Kim, L. Muechler, R. Queiroz, M. Oudah, L. M. Schoop, D. A. Bonn, and S. A. Burke, *Physical Review B*, L121111arXiv:2010.00070.
- [42] M. Gonçalves, P. Ribeiro, E. V. Castro, and M. A. N. Araújo, *Phys. Rev. Lett.* **124**, 136405 (2020).
- [43] For Gaussian distributed disorder, rare regions effects yield, instead, an avoided quantum critical point [57].
- [44] Y. Wang, H. Hu, and S. Chen, *Phys. Rev. B* **98**, 205410 (2018).
- [45] S. M. João and J. M. V. P. Lopes, *Journal of Physics: Condensed Matter* **32**, 125901 (2019).
- [46] S. M. João, M. Andelković, L. Covaci, T. G. Rappoport, J. M. V. P. Lopes, and A. Ferreira, *R. Soc. Open Sci.* **7**, 191809 (2020), arXiv:1910.05194.
- [47] L. Li, C. Yin, S. Chen, and M. A. N. Araújo, *Phys. Rev. B* **95**, 121107 (2017).
- [48] S. S. Pershoguba and V. M. Yakovenko, *Phys. Rev. B* **86**, 075304 (2012).
- [49] W. Shockley, *Phys. Rev.* **56**, 317 (1939).
- [50] D. Vanderbilt, *Berry Phases in Electronic Structure Theory* (Cambridge University Press, 2018).
- [51] J. Silva, E. V., M. A. N. Araújo, P. Ribeiro, and M. Gonçalves, (in preparation).
- [52] J. Hu, Z. Tang, J. Liu, X. Liu, Y. Zhu, D. Graf, K. Myhro, S. Tran, C. N. Lau, J. Wei, and Z. Mao, *Phys. Rev. Lett.* **117**, 016602 (2016).
- [53] J. Hu, Z. Tang, J. Liu, Y. Zhu, J. Wei, and Z. Mao, *Phys. Rev. B* **96**, 045127 (2017).
- [54] R. Li, H. Ma, X. Cheng, S. Wang, D. Li, Z. Zhang, Y. Li, and X.-Q. Chen, *Phys. Rev. Lett.* **117**, 096401 (2016).
- [55] Z. Liu, H. Wang, Z. F. Wang, J. Yang, and F. Liu, *Phys. Rev. B* **97**, 155138 (2018).
- [56] E. Emmanouilidou, B. Shen, X. Deng, T.-R. Chang, A. Shi, G. Kotliar, S.-Y. Xu, and N. Ni, *Phys. Rev. B* **95**, 245113 (2017).
- [57] J. H. Pixley, D. A. Huse, and S. Das Sarma, *Phys. Rev. X* **6**, 021042 (2016).